Polarization weighting of Fano-type transmission through bi-dimensional metallic gratings

Kevin Tetz, Vitaliy Lomakin, Maziar P. Nezhad,* Lin Pang, and Yeshaiahu Fainman

Department of Electrical and Computer Engineering, University of California–San Diego, 9500 Gilman Drive, San Diego MC 0409, California 92093, USA
Corresponding author: maziar@ucsd.edu

Received August 3, 2009; revised December 14, 2009; accepted December 17, 2009; posted February 17, 2010 (Doc. ID 115118); published March 31, 2010

We demonstrate an approach allowing isolating effects of surface plasmon polariton mediated resonant transmission in a periodic grating by means of polarization rotation. The grating comprises a square array of cylindrical holes in an optically thick metallic film. Transmittance data for the co- and cross-polarized cases are described accurately with Fano-type and pure Lorentzian-type line shapes, respectively. This polarization control allows for changing the relative weights of resonant and non-resonant transmission mechanisms, thus controlling the shape and symmetry of the observed Fano-type line shapes.

OCIS codes: 240.6680, 260.3910.

1. INTRODUCTION

Resonant scattering from periodic gratings has been the subject of extensive investigations (see, e.g., [1]). Typically, scattering coefficients of any periodic grating supporting a slow wave, e.g., surface plasmon polaritons (SPPs) or guided waves, are characterized by resonant features. Such features include strong resonant absorption dips in the reflection coefficient, rapid variations of the scattering coefficient phase, and resonant peaks in the magnitude of the transmission coefficient, among others. These features are manifestations of so-called resonant Wood's anomalies [2,3] and they occur approximately when the wave vector of one of the diffraction orders matches that of the slow wave. Mathematically, these anomalies are evident through the presence of complex frequency/angular poles in the scattering coefficient for incident radiation with a given real frequency/angle. When the incident field frequency/angle is scanned through these poles, the scattering coefficient exhibits resonant behavior. In addition to these resonances, a non-resonant field component is always present as well. The superposition of the resonant and non-resonant components results in asymmetry in the shape of the scattering coefficients, resulting in so-called Fano profiles [3–8], which depend on the relation between the magnitude and phase of the resonant and non-resonant components.

The relation between measured resonant and non-resonant components depends not only on the structure parameters, but also on the specific experimental setup. In particular, a linearly polarized field upon scattering from a bi-dimensional grating, i.e., a grating comprising periodicity in two orthogonal dimensions, generates co- and cross-polarized components. Most of the utilized experimental setups implement measurements of co-polarized incident and scattered field components, thus limiting the observed line shapes. SPP mediated polarization rotation effects for one-dimensional gratings in conical mounts [9] have recently been extended to investigate far-field scattering from excited SPP waves in two-dimensional (2-D) nanohole arrays [10–13].

The objective here is to demonstrate experimentally and analytically the dependence of measured intensity through a bi-dimensional periodic grating after analyzing the polarization state of the transmitted optical field for various input polarization states. This is achieved by using an additional polarizer in the scattered field, referred to as an analyzer in the following analysis, which allows control of each of these components of the scattered field and thereby changes the shape of the measured transmitted field. We show that the shape of the resonant transmission depends on the polarization state of the incident field, the excited SPP mode, and the polarization state of the measuring apparatus, enabling the observation of both Fano-type and pure Lorentzian-type line shapes. The particular investigated grating type is a metallic plate perforated by a rectangular array of subwavelength holes. Gratings with scatterers of other shapes and non-square periodicities [14–16] can be handled similarly. The presented ideas and results have a wide applicability to the general theory of scattering from resonant gratings. For example, typically the frequency dependence of the resonant scattering coefficients is associated with red-shifted tails [4–8]. The shape of the scattering coefficient magnitude depends on the relation between both the amplitude and the phase of the resonant and non-resonant components.

The outline of the paper is as follows. Section 2 describes the system under investigation and presents typical spectral dispersion measurements for comparison with those existing in the literature. Section 3 focuses on the analysis and experimental validation of the polarization dependence in transmission near a single isolated resonance, followed by developing a phenomenological model which accounts for this polarization dependence. The measured data are analyzed and compared with the developed model, providing insight into the physics of the

1084-7529/10/040911-7/$15.00

interference of these scattering processes. Conclusions and a brief summary are given in Section 4.

2. EXCITATION OF SPPs IN NANOHOLE ARRAYS

A. Phase Matching for Excitation of SPPs in Metal Films Perforated by 2-D Nanohole Array

The geometry for excitation of a SPP wave on a metallic film perforated with an array of cylindrical holes is shown schematically in Fig. 1. The spectral transmittance of the nanohole arrays has been described recently by a number of authors. An intuitive explanation of the wave phenomena underlying the physics of the transmission through small hole arrays can be given in terms of the SPP excitation [17,18]. An incident electromagnetic wave excites a SPP when the sum of its in plane component of the wave vector and a combination of reciprocal lattice vectors produce a SPP wave vector—that is, when the following phase matching condition is fulfilled:

$$\mathbf{k}^{\mathrm{spp}} = \mathbf{k}_{\parallel} \pm n\mathbf{K}_x^G \pm m\mathbf{K}_y^G, \tag{1}$$

where $\mathbf{k}^{\mathrm{spp}}$ is the SPP wave vector; $\mathbf{K}_x^G$ and $\mathbf{K}_y^G$ are the grating reciprocal lattice vectors in the x- and y-directions, respectively; m and n are integers that describe the various grating orders; and $\mathbf{k}_{\parallel}$ is the in plane component of the incident wave vector, given by

$$\mathbf{k}_{\parallel} = \mathbf{k}_x + \mathbf{k}_y = k_0[\hat{\boldsymbol{x}} \sin\theta \cos\phi + \hat{\boldsymbol{y}} \sin\theta \sin\phi]. \tag{2}$$

Here, $k_0 = 2\pi/\lambda$ is the free space wave vector, ϕ is the polar angle given by $\phi = \tan^{-1}(y/x)$, and θ is the azimuth angle given by $\phi = \cos^{-1}(z)$ (Fig. 1). In a first approximation, we assume a small modulation in the effective index of the structure (valid in the limit $d \ll a$) such that the SPP wave vector can approximately be equal to that of the case of a planar metal surface, with no holes, abutting an adjacent dielectric layer,

$$|\mathbf{k}_{1-2,2-3}^{\mathrm{spp}}| \simeq k_0 \sqrt{\frac{\varepsilon_{1,3}\varepsilon_2}{\varepsilon_{1,3} + \varepsilon_2}}, \tag{3}$$

where ε_1 and ε_3 are the dielectric constants of the incident medium and substrate, respectively. Although there is a number of interesting phenomena which involve the coupling between SPP waves excited on opposing sides of the film (double resonances or "surface plasmon molecules"), we limit our present study to the role of SPPs in enhanced transmittance mediated by its excitation on a single side of the metal film. When the phase matching condition in Eq. (1) is met, the incident field interacts strongly with the SPP and this interaction results in strongly enhanced transmission. The phenomena of resonant transmission can be explained more rigorously as particular manifestations of so-called resonant Wood's anomalies [1,3] that are also associated with Fano profiles. In the framework of the theory of resonant Wood's anomalies, the transmission (scattering) coefficients are represented as a sum of resonant and non-resonant components. Considering the transmission coefficient t either as a function of the parallel wave vector $k_{\parallel}$ for fixed frequency ω and the azimuth component of incident angle, or as a function of frequency ω for a fixed angle of incidence, it is written as [1,3]

$$t(\zeta) = t_b(\zeta) + \sum_{n,m} \frac{c_{nm}}{\zeta - \zeta_{nm}}, \tag{4}$$

with $\zeta \in \{k_{\parallel}, \omega\}$. In Eq. (4), the first and second terms in the right hand side are the non-resonant (background) and resonant components in the transmission coefficient. The resonant component is characterized by complex poles $\zeta_{nm} = \zeta_{nm}^R + j\zeta_{nm}^I$, which satisfy $\zeta_{nm}^R \approx \zeta_{nm}^{\mathrm{res}}$ with $\zeta_{nm}^{\mathrm{res}}$ being frequency/wave vector solutions of Eq. (1), and corresponding residues $c_{nm} = \mathrm{Res}_{\zeta_{nm}}\{t\}$. From Eq. (4), the magnitude of the transmission coefficient exhibits strong peaks for $\zeta \approx \zeta_{nm}^R$ whose width is determined by ζ_{nm}^I which, in turn, is comprised of two components corresponding to the material loss and radiative damping. Physically, the complex frequency poles ω_{nm} characterize resonances, which represent damped exponential fields when the field is excited by a transient source [19]. The complex parallel wavenumber poles $k_{\parallel,nm}$ characterize leaky waves that "radiate" their power out of the perforated plate [2,20–24].

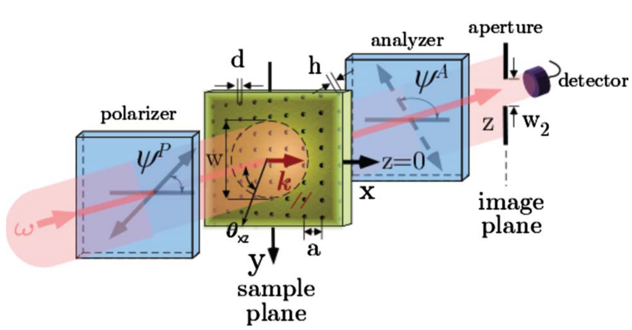

Fig. 1. (Color online) Geometry for excitation of SPP fields on metal films perforated by a 2-D nanohole grating. The inset shows the respective directions as defined in reciprocal lattice space.

B. Spectral Dispersion Mapping for a Single Resonance

In this section we will examine the spectral transmittance through the bi-dimensional nanohole array. We restrict our study to excitation of SPPs on one side of the film only, when $|\mathbf{k}_{1-2}^{\mathrm{spp}}| \gg |\mathbf{k}_{2-3}^{\mathrm{spp}}|$ for any given order (m,n). This assumption means that the frequencies of the lowest order SPP modes excited on the upper and lower interfaces of the metal-dielectric boundaries are well separated in frequency, and therefore there is no coupling between the SPP modes on the opposite sides of the metal film (i.e., under the assumption that the coupling to higher order modes is weak). The experimental samples consist of 100 nm aluminum films on a GaAs substrates perforated by a 2-D array of holes with diameters of $d = 350$ nm and with periods a of 1.2, 1.4, and 1.6 μm. The total perforated area of 200 μm $\times$ 200 μm was used for measurements that followed closely the techniques discussed in [13]. The sample was first aligned normal to the beam axis and the azimuthal angle ϕ was set to a value of either 0 or $\pi/4$ corresponding to the Γ-$\mathbf{X}$ or Γ-$\mathbf{M}$ directions in the reciprocal lattice space. At each azimuthal angle, the polar angle θ (i.e., angle of incidence) was varied from 0 to $7\pi/36$ rad (corresponding to about 35°). The measured dispersion for the three samples with various periods a is shown in Fig. 2(A), displaying the unpolarized (i.e., polarizer/analyzer pair removed) zero-order transmittance for normalized frequency versus normalized in-plane wave vector in both the Γ-**X** and Γ-**M** directions. The data have been normalized by the hole area per unit cell and combined to give a full perspective on the SPP excitation conditions for a large characterization space. The maximum transmission ($\sim 9\%$ for $a = 1.4\ \mu$m and $\sim 13\%$ for $a = 1.2\ \mu$m) occurs at normal incidence for a slightly redshifted wavelength from that corresponding to $a/\lambda = 1.0$.

The data are dominated by the asymmetric Fano-type line shape features, which correlate with resonant transmission by excitation of various SPP wave modes at the various orders (m,n). The essential feature to notice is that the SPP fields are excited at neither the maxima nor the minima of this curve; rather, the interference between the resonant and non-resonant components leads to the dispersive line shape. For these samples, as noted above, only SPP modes on the air–metal (AM) interface are efficiently excited; the first order modes for the semiconductor–air interface occur at much lower frequencies, and the higher order modes that occur at these frequencies are clearly not discernable in these measurements. Dispersion curves shown in Fig. 2(B) are calculated for SPP excitation at the AM interface for a single period ($a = 1.4\ \mu$m) according to Eqs. (1)–(3) and include the frequency dependence of the dielectric constant of aluminum. These curves predict well the frequency of the SPP features for all of the data on the normalized frequency scale. More rigorous methods are required to theoretically determine the relative strength of the coupling as well as the absolute spectral shape of the various bound and propagating modes (i.e., diffraction orders). Qualitatively, however, there have been a number of studies that have succeeded in explaining the effects of the various geometric parameters on the spectral transmittance. The resonant transmission mechanism, as elucidated in [17], consists of coupling to a SPP mode, evanescent transmission through the below-cutoff waveguide hole, and scattering of radiation again from the hole array to produce propagating modes. The hole size, in the long wavelength limit, determines the scattering rate of [8,18] and hence the lifetime of the mode, and increasing size will tend to increase the linewidth of the transmitted radiation. We investigate the polarization dependence of the spectral transmittance of this resonant transmission mechanism more carefully in the next section.

3. POLARIZATION DEPENDENT TRANSMISSION

A. Fixed Angle Rotating Analyzer

In this section we use a slightly different sample than in Section 2. The reason is to facilitate a more careful study of the resonant transmission mechanism. The sample consists of an array of holes in gold film on a silica glass substrate with the geometric parameters $h = 200$ nm,

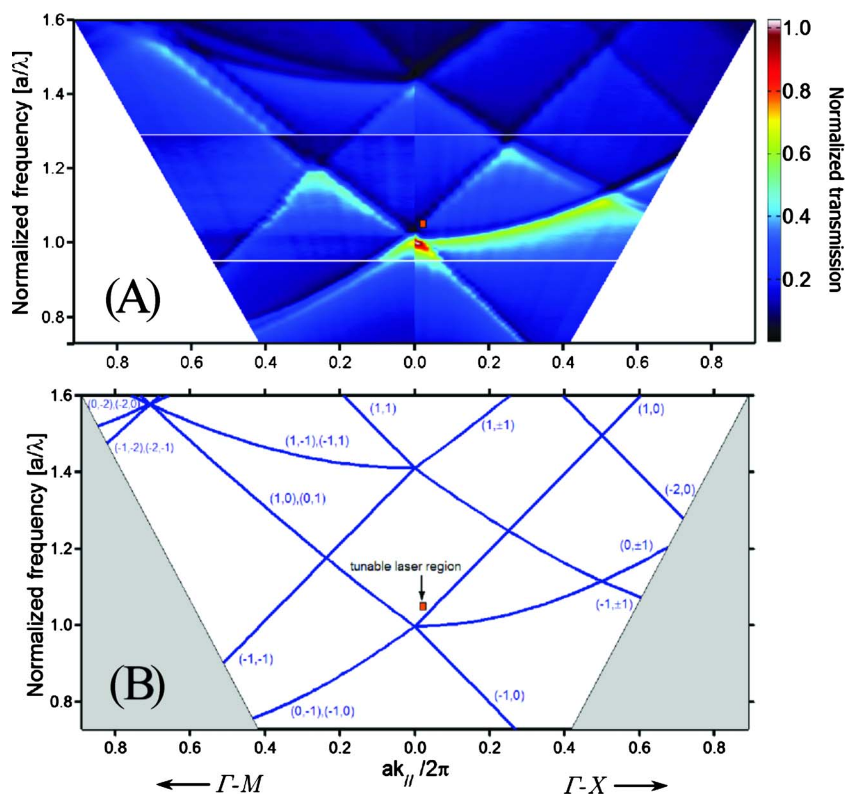

Fig. 2. (Color online) (A) Unpolarized spectral measurements of unpolarized zero-order for cubic arrays of holes in a thin aluminum film on a GaAs substrate. Data from several arrays with different periods a have been combined for these composite intensity images, where the stitching frequencies appear as horizontal white lines. The transmittance has been normalized by the hole area per unit cell. (B) Calculated SPP phase matching conditions for the same parameter space. For comparison, the region corresponding to the high resolution measurements of the gold sample discussed in Section 2 is also shown [small box in (A) and (B)].

$d=200$ nm, and $a=1.63$ μm (see Fig. 1). The Ti adhesion layer of 10 nm is also used to effectively suppress SPP fields on the gold–substrate interface. The details of the fabrication method are discussed in more detail elsewhere [5]. At this point, we will focus on examining the polarization dependence of a single resonant mode, $[+1,\ 0]$. We use a laser with a spectral linewidth much narrower than the SPP resonant transmission linewidth that is tunable in the spectral range of $\lambda=1520-1570$ nm, and will also restrict our SPP measurements to the Γ-$\mathbf{X}$ direction. This parameter space is indicated by the very small shaded regions in Figs. 2(A) and 2(B). For this sample, the film thickness is larger, the hole diameters are smaller, and the divergence of the beam is smaller, all of which lead to narrower measured linewidths than shown in Fig. 2.

The polarization dependent spectral transmission for a fixed value of $\theta=\pi/90$ is shown in Fig. 3. The incident field polarizer angle is set to an angle $\psi^P=\pi/4$, and the output field polarization analyzer angle ψ^A is varied from 0 to 2π in increments of $\pi/36$. Figure 4(A) shows the measured transmittance, showing a Malus-type $\cos^2\psi^A$ dependence across the entire spectral range. These data have been smoothed to remove the effects of reflections from the substrate (which had no anti-reflection coating). To see the underlying structure, we normalize the data along the radial (i.e., normalized frequency a/λ) direction for each value of ψ^A to the maximum of each scan in the radial direction, which is shown in Fig. 3(B).

The transmission maximum is clearly observed to vary with ψ^A—most notably, the white, maximum value, is not circular [see Fig. 3(B)]. This is most clearly evident at $\pi/2$ ($3\pi/2$), where there is a discontinuity in the transmission maximum. Qualitatively, this is a result of a shift due the interaction of the discrete state resonance with the continuum [7]. Moreover, the transmission is never extinguished because of effective polarization rotation by the resonant transmission mechanism. The surface wave is excited by a projection of the incident polarized field, and the propagating surface field interacting with the nanohole array creates a reradiated field which is again projected onto the analyzer. The non-resonant background contribution can be effectively suppressed and in this case the resonant term can be isolated and investigated independently. We address this interesting polarization dependence analytically and quantitatively in the next subsection.

B. Analytical Model for Polarization Dependent Transmission

At this point, we will focus on examining the case of a single resonance in the $[\pm 1,0]$ (i.e., Γ-$\mathbf{X}$) direction. For such a single resonantly excited mode Eq. (4) can be rewritten as

$$t(\zeta)=t_b(\zeta)+\frac{c_n}{\zeta-\zeta_n}. \tag{5}$$

Following the description of [2,3] for a constant background $t_b=t_{b0}$ the expression of Eq. (5) can be written in terms of intensity in the form

$$|t(\zeta)|^2=\frac{(\zeta-\zeta_z^R)^2+(\zeta_z^I)^2}{(\zeta-\zeta_n^R)^2+(\zeta_n^I)^2}|t_{b0}|^2, \tag{6}$$

where $\zeta_{z,n}=\zeta_{z,n}^R+i\zeta_{z,n}^I$, $\zeta_z=\zeta_n-\nu$, and the coefficient ν relates the ratio of the complex amplitudes of the resonant to background transmission coefficients,

$$\nu=\frac{c_n}{t_{b0}}. \tag{7}$$

Next we investigate the variations in the measured line shapes as a function of the various polarization states of the input optical field and the output field resulting from the interaction with the sample and projected onto the output field analyzer. This process can be effectively described using the Jones matrix formalism. The incident linear polarization state is separated into two components consisting of the resonant and the background field contributions to the transmission through the sample, which are recombined at the output producing a field accounting for the relative amplitude and phase of each component. In general, the output field is given by

$$\mathbf{E}_{\mathrm{out}}=\mathbf{R}^{-1}(\psi^A)\mathbf{A}\mathbf{R}(\psi^A)\mathbf{M}^s\mathbf{E}_{\mathrm{in}}(\psi^P), \tag{8}$$

where $\mathbf{M}^s$ is the sample transfer matrix that needs to be determined, $\mathbf{A}=\left(\begin{smallmatrix}1&0\\0&0\end{smallmatrix}\right)$ is the output analyzer, and $\mathbf{R}$ is the rotation matrix for the coordinate system shown schematically in Fig. 1. The incident linearly polarized field is given by $\mathbf{E}_{\mathrm{in}}(z=0^-)=E_0(\hat{\boldsymbol{x}}\cos\psi^P+\hat{\boldsymbol{y}}\sin\psi^P)$. The sample transfer matrix $\mathbf{M}^s$ then takes the form

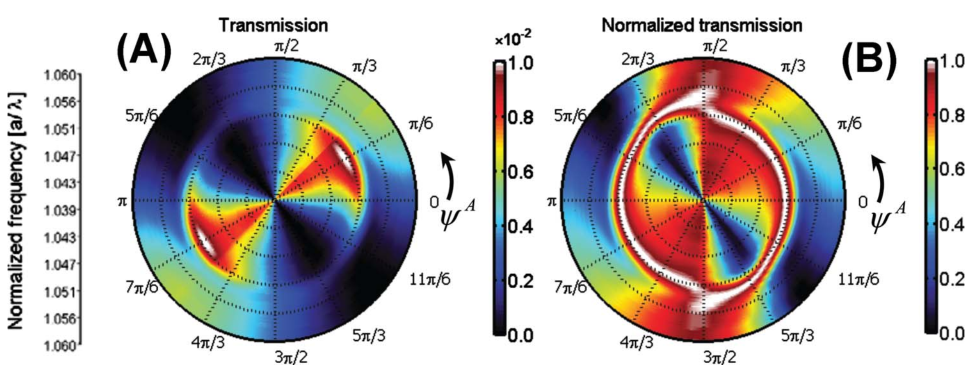

Fig. 3. (Color online) Measured transmission as a function of frequency (radial direction) and analyzer (azimuth angle). Data in (B) are the same as (A); however, it has been normalized along each ψ^A to the maximum of each scan in the radial direction (normalized frequency, a/λ) for viewing the salient properties of the transmission.

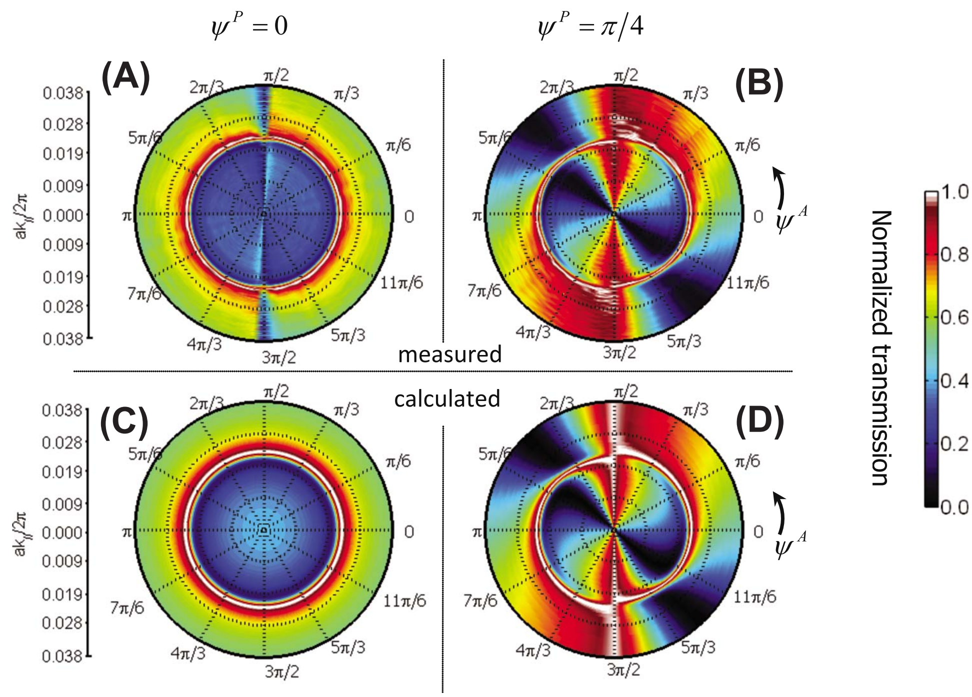

Fig. 4. (Color online) Measured and calculated normalized transmissions as functions of wave vector and ψ^A at fixed frequency for two input polarization states: (A) and (C) are $\psi^P=0$, whereas (B) and (D) are with $\psi^P=\pi/4$. Data have been normalized along the radial direction ($ak_{\parallel}/2\pi$) in the fashion described in Fig. 3. (A) and (B) are the measured data, and (C) and (D) are the calculated values as a fit using the model described in the text.

$$\mathbf{M}_b^s = t'_{b0}\begin{pmatrix} 1 & 0 \\ 0 & 1 \end{pmatrix}, \quad \mathbf{M}_{\text{res}}^s = \begin{pmatrix} c'_n & 0 \\ 0 & 0 \end{pmatrix}, \tag{9}$$

where the subscripts b and res refer to the background and resonant contributions, respectively. Note that the resonantly scattered component results from the excitation and re-radiation of the (1,0)-type mode as indicated by a non-zero element c'_n in the matrix $\mathbf{M}_{\text{res}}^s$. This leads to the two field components behind the film:

$$\mathbf{E}_b(z=0^+) = t'_{b0}E_0(\hat{\boldsymbol{x}} \cos \psi^P + \hat{\boldsymbol{y}} \sin \psi^P),$$

$$\mathbf{E}_{\text{res}}(z=0^+) = \hat{\boldsymbol{x}}c'_nE_0 \cos \psi^P, \tag{10}$$

where $\mathbf{E}_b(z=0^+)$ and $\mathbf{E}_{\text{res}}(z=0^+)$ are the background and the resonant field components behind the sample. Upon the projection of each of these fields onto the output field analyzer and after some simplification, we find that the ratio between the two field components as defined by Eq. (7) yields

$$\nu(\psi^P,\psi^A) = \frac{\hat{\boldsymbol{e}}^A \cdot \mathbf{E}_{\text{res}}}{\hat{\boldsymbol{e}}^A \cdot \mathbf{E}_b} = \frac{c'_n}{t'_{b0}}\frac{1}{(1+\tan \psi^P \tan \psi^A)}. \tag{11}$$

The intensity transmission, then, can be found with Eqs. (6) and (11) with the additional substitution $t_{b0} = t'_{b0} \cos(\psi^A - \psi^P)$ in Eq. (6). This substitution introduces the Malus law dependence and compensates the poles at angles described in Eq. (11).

C. Model Fitting

Figure 4 shows both measured [Figs. 4(A) and 4(B)] and calculated [Figs. 4(C) and 4(D)] transmission intensities as functions of the normalized in-plane wave vector and analyzer angle for a fixed wavelength of $\lambda = 1545$ nm. These data are with the same sample and under the same conditions as that shown in Fig. 3, but with the laser fixed and the angle tuned at different polarization states. Figures 4(A) and 4(C) are for $\psi^P=0$, while Figs. 4(B) and 4(D) correspond to $\psi^P=\lambda/4$. For the data with $\psi^P=0$ [Fig. 4(A)] the measured transmission, when normalized as above, is rotationally invariant in the analyzer angle [except $\psi^A = \pi/2$ ($3\pi/2$), where the measured transmission is below the noise level of our setup detection system]. For the input field set to $\psi^P=\pi/4$, the data are similar to those shown in Fig. 3(B).

For the case when $\psi^P=\pi/2$ (data not shown), the normalized transmission is again invariant with respect to the analyzer angle and nearly constant over this measurement region (the resonant mode is not excited, and thus only the background contribution is present). The resulting fitting parameters for both frequency and wave vector are given in Table 1.

Figure 5 shows single scans of the normalized (to the maximum of each scan) transmittance as a function of parallel wave vector [Fig. 5(A)] and normalized frequency [Fig. 5(B)] for three analyzer angles. For $\psi^A=3\pi/4$ (middle curve), the pure Lorentzian-type line shape is clearly observable. The values of ψ^A are $+\pi/9$ and $-\pi/9$ for curves 1 and 3, respectively, and the two normalized curves display nearly mirror symmetry about the resonance frequency (sketched as dashed red vertical line). This behavior may be understood simply by looking at the relative phase of the two contributions as shown in Fig. 5(C). As the analyzer is rotated about $\psi^A=\pi/4$ ($7\pi/4$), the sign of the projected background component is inverted

Table 1. Fitting Parameters for Normalized Frequency and Normalized Angular Interrogation of Polarization Dependent Transmission

	t'_{b0}	c'_n	ζ_n
$\frac{a}{\lambda}$	$8.15\times10^{-2}-i4.19\times10^{-4}$	$-8.22\times10^{-5}-4.642\times10^{-6}i$	$1.05+i1.32\times10^{-3}$
$\frac{ak_\parallel}{2\pi}$	$1.10\times10^{-3}-i9.82\times10^{-5}$	$1.10\times10^{-3}-i9.82\times10^{-5}$	$2.20\times10^{-2}+i1.20\times10^{-3}$

with respect to the resonant field component. The same situation occurs at $\psi^A=\pi/2$ $(3\pi/2)$; only in this case there the role of the resonant and background contributions is reversed and there is the energy splitting as noted above.

Next we comment on the difference in the shape of the frequency and angular dependence of the transmission coefficient magnitude. For the frequency dependence, the relative positions of ω_n^R and $\omega_{z,n}^R$ are independent of n, the order of the SPP mode. For instance, it is known that when the polarizer and analyzer are co-polarized $\omega_{z,n}^R>\omega_n^R$. On the other hand, for the angular dependence, the relative positions of $k_{\parallel,n}^R$ and $k_{\parallel,z,n}^R$ for mode $n=-1$ are opposite as compared to that for the mode $n=1$. For instance, it is known that for collinear polarizer and analyzer, $k_{\parallel,z,n}^R>k_{\parallel,n}^R$ for $n=-1$ and $k_{\parallel,z,n}^R<k_{\parallel,n}^R$ for $n=1$ [2,23]. An interpretation of this behavior can be given based on the physical meaning of the complex poles ω_n and $k_{\parallel,n}$. The complex frequency poles ω_n always reside above the real axis of the complex ω plane [19]. Therefore, when the resonances are excited by a physical (causal) source, they correspond to a causal time domain signals whose excitation coefficients, viz., the corresponding residues, are taken with the identical sign independently of n. On the other hand the complex poles $k_{\parallel,-1}$ and $k_{\parallel,1}$ correspond to improper (decaying out of plate) and proper (growing out of plate) leaky waves, respectively, since they reside above and below the real axis of the complex $k_\parallel$ plane [2,20–23]. Moreover, these leaky waves are backward and forward waves, viz., waves that have opposite and identical signs of the phase and group velocities [2,20–23]. Therefore, the leaky waves associated with $n=-1$ and 1, when excited by a physical (e.g., point/dipole) source, exist only in the regions $\mathrm{Re}\{k_\parallel\}<k_{\parallel,-1}^R$ and $\mathrm{Re}\{k_\parallel\}>k_{\parallel,1}^R$, respectively, and their excitation coefficients, i.e., corresponding residues, are

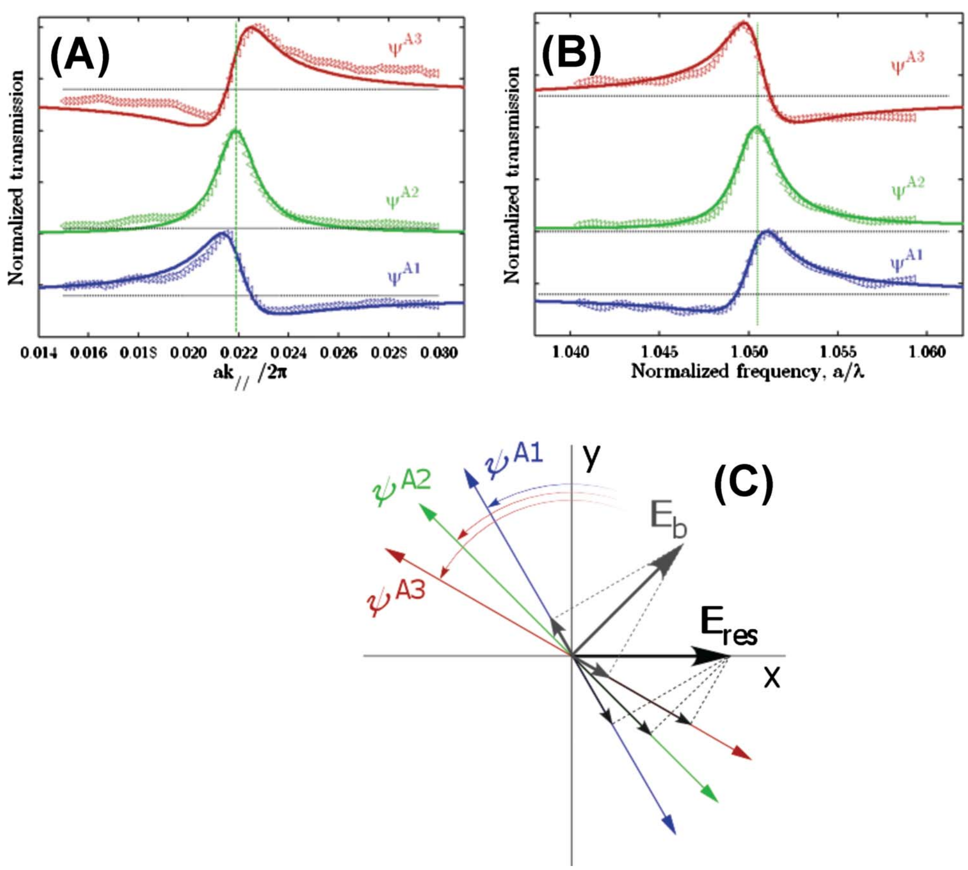

Fig. 5. (Color online) Transmission data for various polarization states demonstrating various Fano type line shapes. Data have been normalized along the radial direction $(ak_\parallel/2\pi)$ and offset vertically for clarity. Dotted lines merely serve as guides to eye. $\psi^{A2}=3\pi/4$, and ψ^{A3} (ψ^{A1}) is $+\pi/9$ $(-\pi/9)$ from this value.

taken into account with opposite sign (as follows from the asymptotic analysis [23,25]). This interpretation is valid not only in the case of collinear but also in the case of cross-polarized analyzer. The latter allows modifying the non-resonant contribution thus modifying the parameter ν, which—in turn—results in the modified symmetry of the shape of the transmission coefficient magnitude in Fig. 5.

4. CONCLUSIONS

In summary, we have presented a detailed high resolution study of the polarization properties in spectral transmittance of a nanohole array grating in a metal film. To describe the measured data, we have extended the explanation of transmission through nanohole arrays in terms of Fano-type line shapes resulting from the coherent interference between a discrete and a continuum of states. In particular, we have shown that these components may be weighted—in amplitude and phase—by control of polarization, resulting in Fano-type lines with various symmetries and detuning values.

While we have shown results for the specific case of a single $[+1, 0]$-type order, and derived an analytical expression which fit our measured results quite well, a similar analysis may be applied to any of the various resonant orders, generalized or applied to periodic structures of different symmetries. It will be of further interest to investigate similar structures at higher frequencies, toward the plasma frequency, where localized surface plasmons and related effects become more pronounced [7].

ACKNOWLEDGMENTS

We gratefully acknowledge support from the National Science Foundation (NSF) and the Defense Advanced Research Projects Agency (DARPA) Center for Optofluidic Integration.

REFERENCES

1. Focus Issue: "Extraordinary Light Transmission Through Sub-Wavelength Structured Surfaces," Opt. Express **12**, 3618–3706 (2004).
2. A. Hessel and A. A. Oliner, "A new theory of Wood's anomalies on optical gratings," Appl. Opt. **4**, 1275–1298 (1965).
3. M. Sarrazin, J. P. Vigneron, and J. M. Vigoureux, "Role of Wood's anomalies in optical properties of thin metallic films with a bi-dimensional array of subwavelength holes," Phys. Rev. B **67**, 085415 (2003).
4. C. Genet, M. P. van Exter, and J. P. Woerdman, "Fano-type interpretation of red shifts and red tails in hole array transmission spectra," Opt. Commun. **225**, 331–336 (2003).
5. K. A. Tetz, L. Pang, and Y. Fainman, "High-resolution surface plasmon resonance sensor based on linewidth-optimized nanohole array transmittance," Opt. Lett. **31**, 1528–1530 (2006).
6. F. J. García de Abajo, J. J. Sáenz, I. Campillo, and J. S. Dolado, "Site and lattice resonances in metallic hole arrays," Opt. Express **14**, 7–18 (2006).
7. S. H. Chang, S. K. Gray, and G. C. Schatz, "Surface plasmon generation and light transmission by isolated nanoholes and arrays of nanoholes in thin metal films," Opt. Express **13**, 3150–3165 (2005).
8. D. S. Kim, S. C. Hohng, V. Malyarchuk, Y. C. Yoon, Y. H. Ahn, K. J. Yee, J. W. Park, J. Kim, Q. H. Park, and C. Lienau, "Microscopic origin of surface-plasmon radiation in plasmonic band-gap nanostructures," Phys. Rev. Lett. **91**, 143901 (2003).
9. S. J. Elston, G. P. Bryanbrown, and J. R. Sambles, "Polarization conversion from diffraction gratings," Phys. Rev. B **44**, 6393–6400 (1991).
10. E. Altewischer, M. P. van Exter, and J. P. Woerdman, "Polarization analysis of propagating surface plasmons in a subwavelength hole array," J. Opt. Soc. Am. B **20**, 1927–1931 (2003).
11. K. A. Tetz, R. Rokitski, M. Nezhad, and Y. Fainman, "Excitation and direct imaging of surface plasmon polariton modes in a two-dimensional grating," Appl. Phys. Lett. **86**, 111110 (2005).
12. E. Altewischer, X. Ma, M. P. van Exter, and J. P. Woerdman, "Fano-type interference in the point-spread function of nanohole arrays," Opt. Lett. **30**, 2436–2438 (2005).
13. R. Rokitski, K. A. Tetz, and Y. Fainman, "Propagation of femtosecond surface plasmon polariton pulses on the surface of a nanostructured metallic film: space-time complex amplitude characterization," Phys. Rev. Lett. **95**, 177401 (2005).
14. R. Gordon, A. G. Brolo, A. McKinnon, A. Rajora, B. Leathem, and K. L. Kavanagh, "Strong polarization in the optical transmission through elliptical nanohole arrays," Phys. Rev. Lett. **92**, 037401 (2004).
15. M. Sarrazin and J. P. Vigneron, "Polarization effects in metallic films perforated with a bi-dimensional array of rectangular subwavelength holes," Opt. Commun. **240**, 89–97 (2004).
16. Y. M. Strelniker, "Theory of optical transmission through elliptical nanohole arrays," Phys. Rev. B **76**, 085409 (2007).
17. W. L. Barnes, W. A. Murray, J. Dintinger, E. Devaux, and T. W. Ebbesen, "Surface plasmon polaritons and their role in the enhanced transmission of light through periodic arrays of subwavelength holes in a metal film," Phys. Rev. Lett. **92**, 107401 (2004).
18. R. Muller, V. Malyarchuk, and C. Lienau, "Three-dimensional theory on light-induced near-field dynamics in a metal film with a periodic array of nanoholes," Phys. Rev. B **68**, 205415 (2003).
19. V. Lomakin and E. Michielssen, "Transmission of transient plane waves through perfect electrically conducting plates perforated by periodic arrays of subwavelength holes," IEEE Trans. Antennas Propag. **54**, 970–984 (2006).
20. R. E. Collin and F. J. Zucker, *Antenna Theory Part 2* (McGraw-Hill, 1969).
21. F. Falco, T. Tamir, and K. M. Leung, "Grating diffraction and Wood's anomalies at two-dimensionally periodic impedance surfaces," J. Opt. Soc. Am. A **21**, 1621–1634 (2004).
22. D. R. Jackson, A. A. Oliner, T. Zhao, and J. T. Williams, "Beaming of light at broadside through a subwavelength hole: leaky wave model and open stopband effect," Radio Sci. **40**, RS6S10 (2005).
23. S. Zhang and T. Tamir, "Spatial modifications of Gaussian beams diffracted by reflection gratings," J. Opt. Soc. Am. A **6**, 1368–1381 (1989).
24. V. Lomakin and E. Michielssen, "Beam transmission through periodic sub-wavelength hole structures," IEEE Trans. Antennas Propag. **55**, 1564–1581 (2007).
25. L. B. Felsen and N. Marcuvitz, *Radiation and Scattering of Waves* (IEEE, 1994).